ISSN 1349-1121
JAXA-RM-12-006E

JAXA Research and Development Memorandum

Effect of Thermodynamic Parameter on Cavitation in Rocket Inducer

Yoshiki YOSHIDA, Kengo KIKUTA, Kazuki NIIYAMA, Satoshi WATANABE

January 2013

Japan Aerospace Exploration Agency

Effect of Thermodynamic Parameter on Cavitation in Rocket Inducer*

Yoshiki YOSHIDA[*1], Kengo KIKUTA[*2]
Kazuki NIIYAMA[*3] and Satoshi WATANABE[*4]

ロケット用インデューサのキャビテーションに与える熱力学的パラメータの影響*

吉田義樹[*1], 菊田研吾[*2]
新井山一樹[*3], 渡邉 聡[*4]

ABSTRACT

Cavitation is physically “a vaporization of liquid” which needs latent heat for phase change. A cavity grows in the liquid, so the latent heat of vaporization can only be supplied by the liquid surrounding the cavity. Thus, the liquid close to the interface region of the cavity is cooled down.

In general, cryogenic liquids are very thermosensitive. For liquid hydrogen and oxygen used in rocket propulsion, the temperature in the cavity, i.e., the vapor pressure in the cavity, is lower than those of the liquid bulk. Thanks to this thermal effect, cavitation in cryogenic liquids is less developed than that in water at room temperature. This thermal effect on cavitation is beneficial in that it improves cavitation performance and alleviates cavitation instabilities in space inducers.

In previous works, we investigated the relationship between the thermodynamic effect and the cavitation instabilities, e.g., rotating cavitation and cavitation surge, with a focus on the cavity length as an indication of cavitation. In the present work, first, aspects of cavitation in an inducer were observed by direct optical visualization in liquid nitrogen. Second, joint experiments in liquid nitrogen and cold water were conducted on a cavitaing inducer. In nitrogen experiments, operating conditions, i.e., rotational speed and liquid temperature, were varied to determine the cavitation scaling law. Through these experimental results, characteristic times, namely, the transit time for bubble growth and the characteristic thermal time introduced from the thermal property, were investigated as a cavitation thermodynamic parameter. It was found out that the adjustment of cavitation number has a good correlation with the ratio of the transit time and the characteristic thermal time.

* Received 3 December 2012
*1 Space Transportation Propulsion Research and Development Center, Space Transportation Mission Directorate
(宇宙輸送ミッション本部　宇宙輸送系推進技術研究開発センター)
*2 Space Transportation Propulsion Research and Development Center, Space Transportation Mission Directorate
(宇宙輸送ミッション本部　宇宙輸送系推進技術研究開発センター)
Present affiliation : IHI Corporation, Aero-Engine & Space Operations
(（株）IHI、航空宇宙事業本部)
*3 Space Transportation Propulsion Research and Development Center, Space Transportation Mission Directorate
(宇宙輸送ミッション本部　宇宙輸送系推進技術研究開発センター)
Present affiliation : Kanazawa Institute of Technology, Department of Mechanical Engineering
（金沢工業大学工学部）
*4 Kyushu University, Department of Mechanical Engineering
（九州大学工学研究院）

INTRODUCTION

Pioneering works of the thermodynamic effect on cavitation performances were conducted by Stepanoff [1] and Cooper [2], who used B-factor ($B=V_v/V_l$) as a thermal cavitaion criterion to explain the difference of NPSH requirement between water and other liquids. Stepanoff investigated the thermodynamic effect on cavitation with regard to the reduction of pump performance (i.e., the measurable cavitation effect of head breakdown $\Delta\psi/\psi_o$ = 3%) as an indication of cavitation. Figure 1 shows that the explanation of Stepanoff's NPSH adjustment Δh_t, where C_1 and C_2 are 3% head breakdown as the reduction of pump performance. Stahl et al. [3] assumed that "the same value of $B=V_v/V_l$ would mean the same extent of cavitation condition and the same damage to the performance." Furthermore, Stepanoff proposed that "such reductions of NPSH values below their cold water test values will be referred to as 'NPSH adjustments' rather than 'NPSH corrections'- an obvious misnomer." In other words, Stepanoff's classical B-factor could be understood as a non-dimensional temperature parameter $B=\Delta T/\Delta T^*$, in which ΔT is the temperature difference between the liquid at infinity and the cavitating region, and $\Delta T^* = \rho_v L/\rho_l C_{pl}$ which depends only upon the fluid property is the characteristic temperature difference by simple heat balance.

Brennen [4] proposed the thermodynamic parameter Σ (Eq. (1)) from the analysis of the dynamics of a single sphere bubble based on the assumption that heat transfer to the interface between a bubble and the surrounding liquid occurs due to the conductive nature. This thermodynamic parameter Σ has the units of $m/s^{3/2}$. Figure 2 shows the thermodynamic parameter Brennen's Σ vs. non-dimensional temperature T/T_c (T_c: critical temperature), Σ increases at an exponential rate in water and other liquid when the temperature increases to near the critical temperature.

$$\Sigma = \frac{(\rho_v L)^2}{\rho_l^{\,2} C_{pl} T_\infty \sqrt{\alpha_l}} \tag{1}$$

Figure 2 shows the thermodynamic parameter Brennen's Σ vs. non-dimensional temperature T/T_c (T_c: critical temperature), Σ increases at an exponential rate in water and other liquid when the temperature increases to near the critical temperature. Furthermore, Brennen [5] considered the time scale of the thermal effect on cavity growth. He introduced the comparison between the transit time $1/\phi\Omega$ (an approximation of transit time of bubble passing through the pump, ϕ: coefficient of flow rate, Ω: rotational speed) and the critical thermal time t_c. The critical thermal time t_c means the least time until the influence of the heat transfer on evaporation appears. He also organized the ratio of the critical cavitation number $\sigma_x/(\sigma_x)_0 = 1 - 2\beta(\Sigma^{**})^2$ (σ_x is the head break cavitation number in thermosensitive fluid, and $(\sigma_x)_0$ is the head break cavitation number in the absence of any thermal effect, e.g., in water) by using the modified non-dimensional thermodynamic parameter $\Sigma^{**} = \Sigma \Big/ \left\{R_T^{\,2}\Omega^3\phi(\sigma_x)_0\right\}^{\frac{1}{2}}$. The arbitrary parameter $\beta = 5 \times 10^{-6}$ was chosen based on many experimental results presented in his textbook (Brennen [5]) in Fig.

3. Thermodynamic effect for pump performance appears over the range of $\Sigma^{**} > 10$, and the cavitation number σ_x is seemed to reach 0 at the range of $\Sigma^{**} > 10^2$-10^3.

Kato [6] also introduced a very similar thermodynamic parameter, $\alpha = \sqrt{\rho_l / \rho_v}\Sigma$ (m/s$^{3/2}$), although his model considered an attached sheet cavity. He rearranged a large number of Hord's experimental results [7] and found a good correlation between the non-dimensional thermodynamic parameter $Y = \alpha\sqrt{C/U^3}$ and the non-dimensional pressure drop ΔC_p inside the cavity in Fig.4, where C was a reference length and U was a reference velocity. Figure 4 shows that the non-dimensional pressure drop ΔC_p increases lineally as increasing of the non-dimensional thermodynamic parameter $Y = \alpha\sqrt{C/U^3}$.

Furthermore, Watanabe et al. [8] proposed a non-dimensional thermodynamic parameter, $\Sigma^* = \Sigma\sqrt{C/U^3}$, from two-dimensional cascade analysis with consideration of the thermodynamic effect. The analyses of Kato and Watanabe indicate that the thermodynamic effects increase with Y / Σ^*, i.e., when fluid temperature is higher and flow velocity is lower. Reference velocity U influences non-dimensional thermodynamic parameters Y / Σ^* of Kato and Watanabe by -1.5th power. The trend of Watanabe's analyzed results for the cavity growth and onset of the cavitation instabilities in a 2D inducer agreed well with the 3D inducer experimental results by Franc et al. [9] and Yoshida et al. [10]. In heat transfer models of Kato and Watanabe, however, the heat transfer was obliged to significantly increase the liquid thermal diffusivity to obtain reasonable predictions because heat transfer at the cavity interface might be greatly enhanced by turbulence flow.

Franc et al. [11] [12] also proposed another non-dimensional thermodynamic parameter, τ/τ_T, from the modified Rayleigh-Plesset equation with consideration of the thermodynamic effect. In the model of Franc, the heat transfer at the babble wall is supposed to be of convective nature. The non-dimensional thermodynamic parameter τ/τ_T of Franc can be physically understood as a ratio of two characteristic times, one being the transit time $\tau=C/U$ and second being the characteristic thermal time $\tau_T = Nu\sqrt{\alpha_l}/\Sigma$, which contains information on heat transfer as the Nusselt number, Nu, at the interface of the cavity.

Recently, several experiments using thermosensitive fluid, i.e., refrigerant R114, hot water, and liquid nitrogen, have been conducted by Franc et al. [9] [12], Cervone et al. [13], and Kikuta et al. [14] [15], to investigate the relationship between thermodynamic effects and cavitation performances/instabilities in space inducers, respectively. They focused on "cavity length" as an indication of cavitation instead of "the reduction of pump performance of Stepanoff ." In general, their experiment results showed that the thermodynamic effects for cavitation performances/instabilities in cavitating inducers increase significantly when the fluid temperature is higher and the rotational speed is lower. Figure 5 (a) and (b) show the typical example of thermodynamic effect on cavitation performance/instability in liquid nitrogen with the length of tip leakage vortex cavitation of each blade as the indication of cavitation [16]. In case of cold liquid nitrogen (T=74 K in Fig.5 (a)), strong Super-SRC (super-synchronous rotating cavitation), SRC (synchronous rotating cavitation) and weak Sub-SRC (sub-synchronous rotating cavitation) appear. To the contrary, in case of hot liquid nitrogen (T=83 K in

Fig.5 (b)), Super-SRC (super-synchronous rotating cavitation) doesn't change at all, however SRC (synchronous rotating cavitation) is weakened considerably and Sub-SRC (sub-synchronous rotating cavitation) diappears. Then, the cavitation performance curve shifts to the left, i.e., lower cavitation numbers caused by the thermodynamic effect.

Several simulation results of a cavitating inducer in hydrogen with thermal effect have been reported. Hosangadi et al. [17] analyzed the classical helical flat plate inducer of NASA (Ball et al. [18]) using their CRUNCH CFD ®code in Fig. 6. Their simulation results showed that the fundamental differences between water and liquid hydrogen and the cavitating performance in liquid hydrogen could be predicted well. In their simulation, temperature depressions of 0.5-1.0 K in the cavity were observed for an inlet reference temperature of 20.55 K with an inducer tip speed U= 130 m/s at a rotational speed of 20000 rpm.

Goncalves et al. [19] have also analyzed another helical flat plate inducer of NASA (Meng et al. [20]) using their FINE/TURBO™ solver integrated the thermal cavitation model in Fig. 7. Their simulation conditions were an inlet reference temperature of 19 K / 23 K and an inducer tip speed U= 198 m/s at a rotational speed of 30000 rpm. Their simulation results were somewhat out of the ordinary. Although the temperature depression in the cavity due to the vaporization cooling effect was about 1 K, the rise of the wall temperature reached 2 K due to the viscous heating effect. This opposite behaviour might possibly have a significant influence on the thermodynamic effect on cavitation in an ultra high-speed hydrogen inducer.

In the present work, the thermodynamic effect on cavitating inducers was investigated by both experiments in cold water and liquid nitrogen. The thermodynamic effect is almost zero in water at room temperature, but can be significant in liquid nitrogen. The influences of rotation speed, Ω, and fluid temperature, T_∞, on cavity growth were investigated in liquid nitrogen and analyzed by comparison of the transit time $\tau=C/U$ and the characteristic thermal time $\tau_T = Nu\sqrt{\alpha_l}/\Sigma$ to examine the cavitation scaling law with the thermodynamic effect.

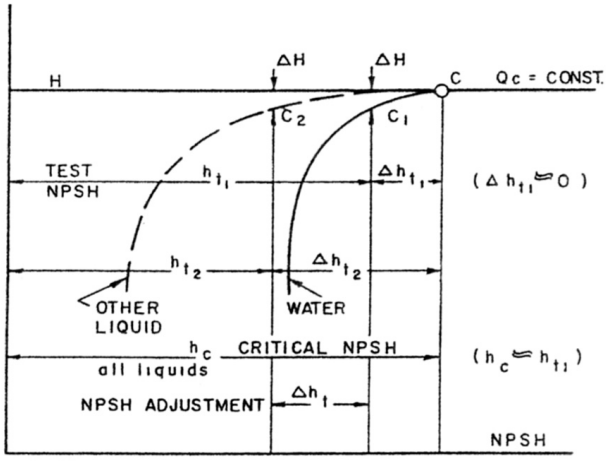

Fig. 1 Cavitation test on two liquids (water and other liquid), explanation of Stepanoff's NPSH adjustment Δh_t, where C_1 and C_2 are 3% head breakdown as the reduction of pump performance from [1]

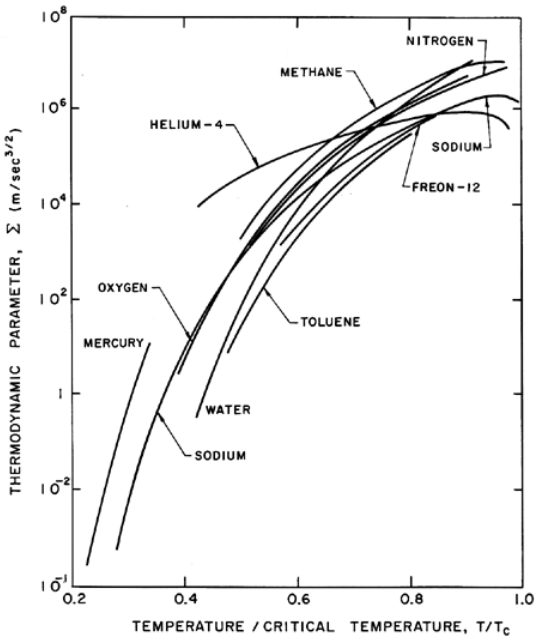

Fig. 2 Thermodynamic parameter Brennen's Σ vs. non-dimensional temperature T/T_c (T_c: critical temperature) from [4]

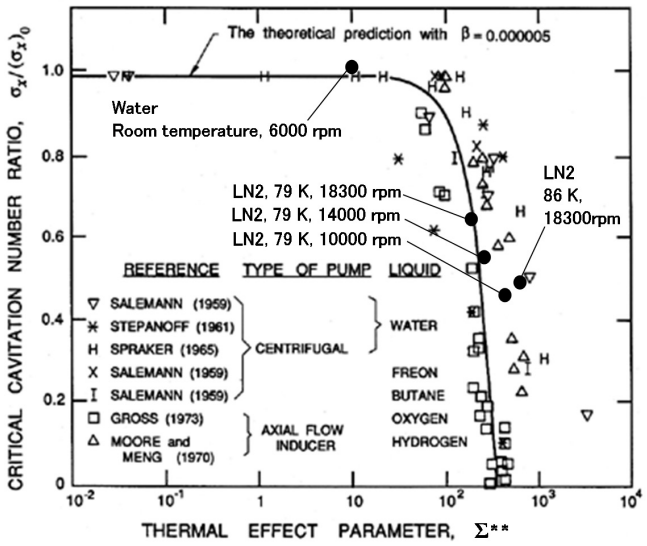

Fig. 3 Critical cavitation number ratio $\sigma_x/(\sigma_x)_0$ vs. non-dimensional thermodynamic parameter Brenenn's Σ from [5] . Including the various present data (●) in Table1**

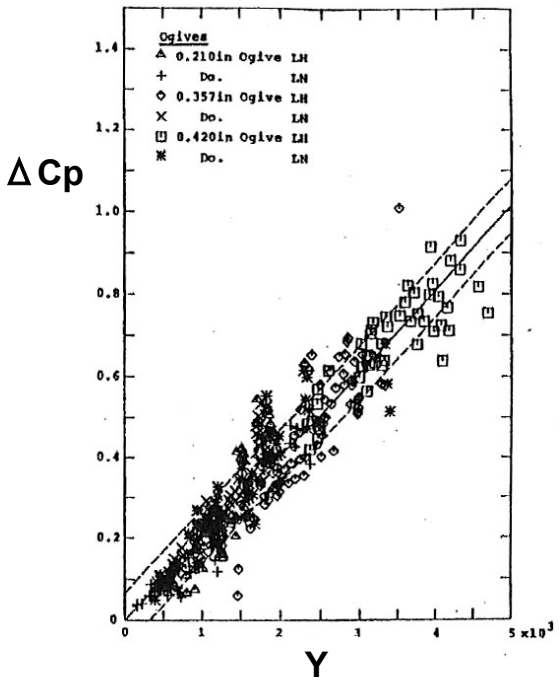

Fig. 4 Non-dimensional pressure drop ΔCp vs. non-dimensional thermodynamic parameter Kato's Y-factor for three ogives in liquid hydrogen and liquid nitrogen from [6]

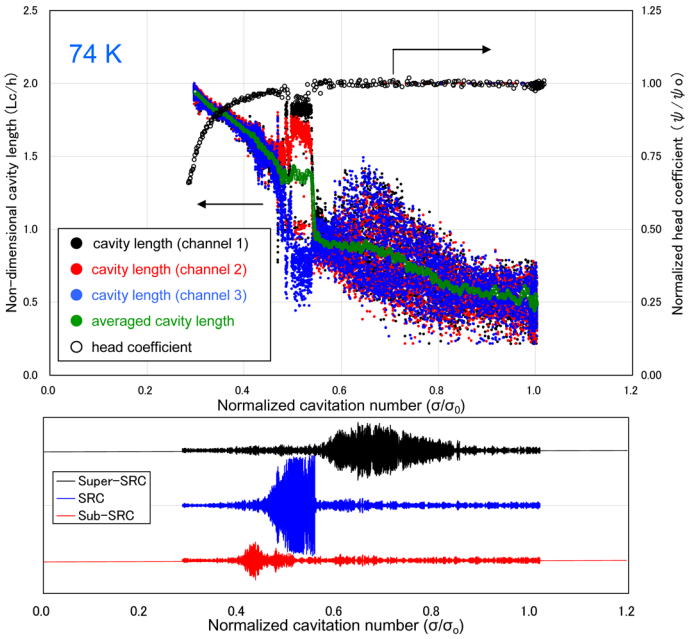

Fig. 5 (a) Cavitation performances and cavity length of each channel and averaged cavity length (top), pressure fluctuations (bottom) for liquid nitrogen 74 K

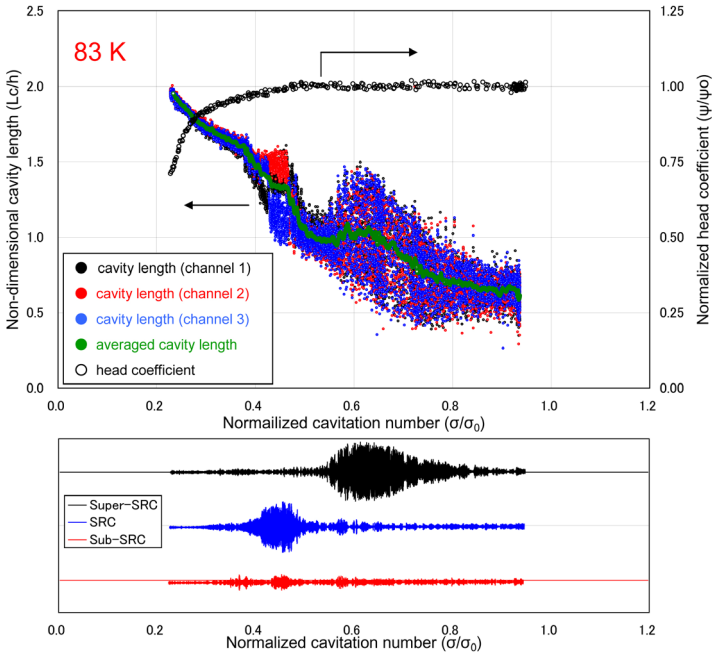

Fig. 5 (b) Cavitation performances and cavity length of each channel and averaged cavity length (top), pressure fluctuations (bottom) for liquid nitrogen 83 K

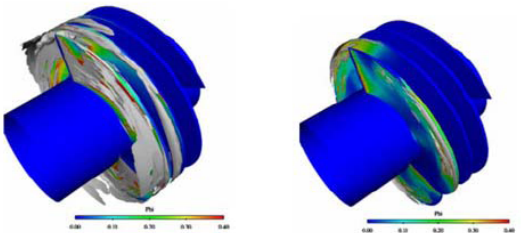

(a) Water (b) Liquid hydrogen

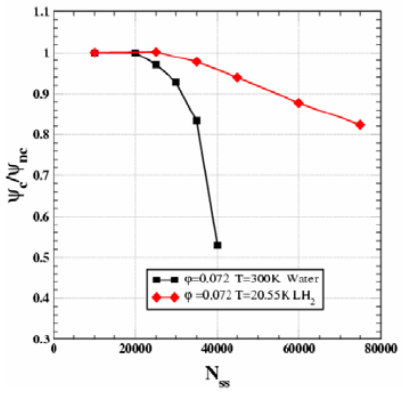

(c) Predicted suction performance

Fig. 6 Isosurface of vapor volume fraction in (a) water, (b) liquid hydrogen, and (c) predicted suction performance for water and liquid hydrogen from [17]

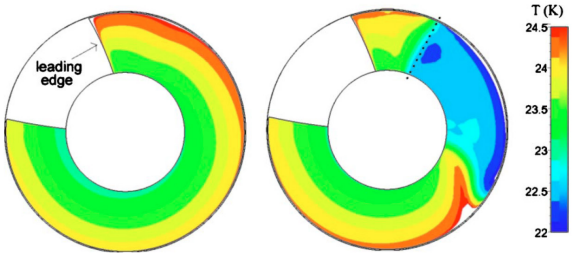

(a) No cavitating (b) Cavitating NPSH=48m

Fig. 7 Wall temperature on sucion side of inducer blade for liquid hydrogen, (a) no cavitating, (b) cavitating NPSH=48m, T_{ref} =23 K from [19]

EXPERIMENTAL BACKGROUND

(1) Aspect of cavitating inducer

Figure 8 presents typical visualization of a cavitating inducer with the same size and shape in both Fig. 8 (a) cold water (306 K) and Fig. 8 (b) liquid nitrogen (79 K) at the same rotation speed of 6000 rpm, the same flow rate, and the same inlet cavitation number (Watanabe et al. [21]). Figure 8 (c) shows the direct visualization in liquid nitrogen from the inception of tip cavitation to the head breakdown at various cavitation numbers, and test facility for the visualization. In this case, non-dimensional thermodynamic parameter was τ/τ_T = 0.01 in water, and τ/τ_T = 15.4 in liquid nitrogen, the latter being much larger than the former. Thus, the thermodynamic effect is expected to be large in liquid nitrogen. It is apparent that the cavitation aspect is quite different in the two liquids. While the water cavities are relatively clear and well defined, the nitrogen cavities are indistinct consisting of many fine bubbles. Sarosdy and Acosta [22] compared the cavitation aspect in water and in Freon 113 using a cavitating disk. They noted that the cavity in Freon was “frothy” as opposed to “glassy” in water. From the visualization of Fig. 8 (a) and (b), it seems likely that the cavity is “creamy” in nitrogen as opposed to “icy” in water.

Furthermore, it can be observed that the cavity length of tip leakage vortex cavitation along the blade in liquid nitrogen is shorter than that in water. This tendency is the same as the difference of the length of leading edge cavitation between refrigerant R114 and water of Franc’s visualization of cavitating inducer in Fig. 9. The length of the leading edge cavitation in refrigerant R114 was shorter than that in water even at the same cavitation number (Franc et al. [9] [12]).

From these visualizations and Hosangadi’s CFD results [23], we conjecture that the frothiness of cavity in thermosensitive fluid may be attributed to the lower volume fraction in the cavity that reduces the density difference. Consequently, the cavity is more porous in thermosensitive fluid than in water. Thus, the flow does not turn rapidly when the liquid streamlines flow into the cavity in Fig. 10. This is assumed to be one of the reasons why inducer cavitation instabilities are suppressed in thermosensitive fluid, because it is well known that the origin of rotating cavitation is the change of the streamline caused by the interaction between the cavity closure and the incidence at the leading edge of the adjacent blade (Horiguchi et al. [24]). Recently, rotating cavitaions have been simulated in several CFD analyses. Iga et al. [25][26], AN et al. [27] and Tani et al. [28] discussed the propagating mechanism of rotating cavitation.

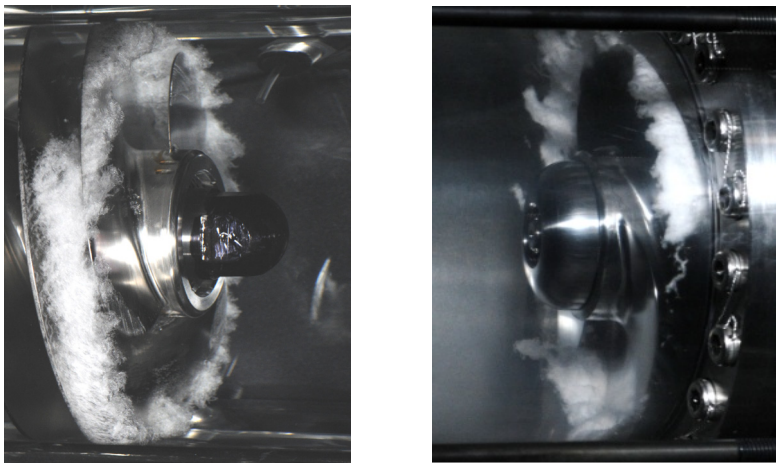

(a) Water (b) Liquid nitrogen

Fig. 8 (a), (b) Visualization of cavitating inducer in (a) water (306 K) and (b) liquid nitrogen (79 K) for the same cavitation number, the same rotational speed, and the same flow rate.

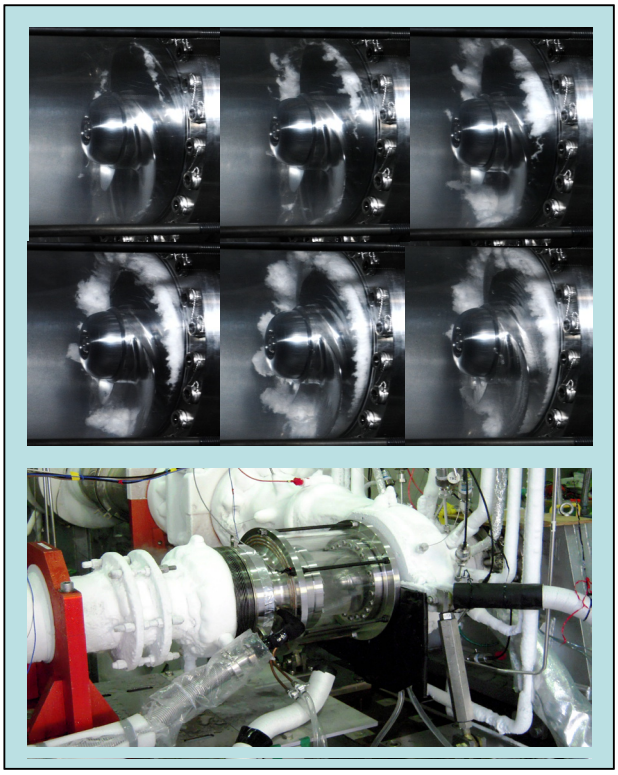

Fig.8 (c) Direct visualization of cavitating inducer in liquid nitrogen, from the inception of tip cavitation to the head breakdown at various cavitation numbers, and test facility for the visualization from [21]

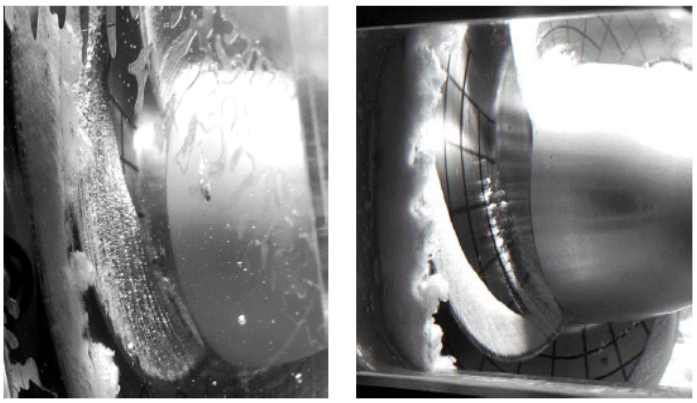

(a) Water (room temperature) (b) Refrigerant 114 (40 ℃)

Fig. 9 Visualization on cavitating inducer with leading edge cavitation in (a) water (at room temperature) and (b) refrigerant 114 (at 40 ℃) for the same cavitation number, the same rotational speed, and the same flow rate from [12]

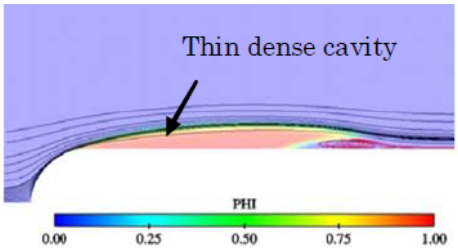

(a) isothermal case

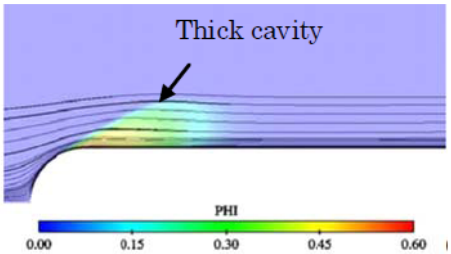

(b) With thermodynamic effect

Fig. 10 Vapor volume fraction contours and streamlines for liquid nitrogen cavitating flow around a ¼ caliber headform, (a) isothermal case, (b) with thermodynamic effect from [23]

(2) Temperature depression of leading edge cavitation on hydrofoil

Franc et al. [29] succeeded in a challenging experiment of direct measurement of the temperature depression on a rotating inducer in refrigerant R114 at room temperature in Fig. 11. Temperature depression ΔT in the cavity increases as decreasing of the inducer cavitation number. However, direct measurement of the temperature depression on a rotating blade is more difficult in cryogenic fluid. Recently, Cervone et al. [30] and Gustavsson et al. [31] used an NACA0015 hydrofoil to investigate the thermodynamic effect using hot water and Fluoroketone as working fluid, respectively. Figure 12 shows that cavitation appearance in (a) cold water T=25℃, α=4 deg., σ=1.25, and (b) hot water T=70℃, α=8 deg., σ=2.0 from [30]. In case of hot water of Fig. 12 (b), cavity bubbles are smaller than those of cold water in Fig. 12 (a).

We directly measured the temperature depression of the leading edge cavitation on a hydrofoil in liquid nitrogen (Niiyama et al. [32]). The experiments were conducted in the Cryogenic Cavitation Tunnel (CCT) (Niiyama et al. [33]) of the Japan Aerospace Exploration Agency (JAXA) in Fig.13. An NACA16-012 hydrofoil with a chord length of 48 mm was installed in the test section with an angle of attack 8 degrees. For the NACA16-012 hydrofoil, Franc and Michel [34] observed many kinds of cavitations in detail. Five miniature diode sensors (LakeShore Cryotronics, Inc., DT-670-SD) were mounted on the suction side of the hydrofoil from the leading edge to the trailing edge to measure the temperature of cavity bubbles. The free-stream temperature of the liquid nitrogen was 90.4 K, the free-steam velocity was U ≈13 m/s, and consequently, the non-dimensional thermodynamic parameter was $\tau/\tau_T \approx 6 \times 10^2$. This value is much greater than that of the inducer observation mentioned above. Thus, the thermodynamic effect is expected to be much larger.

Figure 14 shows the aspects of cavitating flow on the hydrofoil at several cavitation numbers. The inception of cavitation occurs just at the leading edge in Fig. 14 (a), and then the cavity bubbles gradually expand to the trailing edge as cavitation number decreases in Fig. 14 (b) - (d). We confirmed that the cavity consisted of many tiny bubbles, and that sheet cavitation could not be observed anywhere. Although this aspect of the cavitation in the liquid nitrogen is quite different to the cavitation observed in water (Franc and Michel [34]), similar aspects were also observed in other thermosensitive fluids (Cervone et al. [30] and Gustavsson et al. [31]). Furthermore, this aspect is similar to the cavitation in the inducer in liquid nitrogen mentioned above.

On the other hand, the cavity length did not oscillate when the cavity length developed over chords of 0.5-0.7C, although cavitation oscillations caused by the re-entrant jet were observed in a usual water hydrofoil (Kawanami et al. [35], Watanabe et al. [36]). Cavitation instabilities caused by the re-entrant jet were perfectly suppressed due to the thermodynamic effect on cavitation. The reason why the cavitation instabilities didn't occur in the liquid nitrogen might be explained as follows [37]. Because the surface tension of the liquid nitrogen (6.1 mN/m @90.4K) is much smaller than that of cold water (71.7 mN/m @300K), a lot of cavitation bubbles with small radius can incept in the liquid nitrogen. However, the

growth of the bubble is very slow caused by the strong thermodynamic effect ($\tau/\tau_T \approx 6 \times 10^2$) in the hot liquid nitrogen. Therefore, the bubbles could not develop considerably, and not join together. As the result, No sheet cavitation could be formed in the liquid nitrogen. Although the cavity cloud in liquid nitrogen looks like as "cream" consisted of tiny cavitation bubbles, the void fraction might be very low. Conversely, in water, "icy" cavitation bubble joint together and can be formed to clear sheet cavitation, in which the void fraction is almost 1.0. The sheet cavitation causes the cavitation instability related to the re-entrant jet in water [35].

Figure 15 shows variation of the non-dimensional temperature depression $B=\Delta T/\Delta T^*$ measured by each temperature sensor against the cavitation number σ. In the present experiment, ΔT^*=1.8 K at the freestream temperature T_∞= 90.4 K (T^*=0.43) of liquid nitrogen. For reference, the variation of the characteristic temperature difference $\Delta T^* = \rho_v L/\rho_l C_{pl}$ of themosensitive fluids compared with water are presented against the non-dimensional temperature $T^* = (T-T_t)/(T_c-T_t)$ in Fig. 16. The characteristic temperature difference $\Delta T^* = \rho_v L/\rho_l C_{pl}$ depends only upon the fluid temperature. For cryogenic fluids, the saturation temperatures at the ambient pressure are considerably farther from the temperatures at the triple point than that in cold water. Thus, the liquid-vapour density ratio is lower, and consequently, more liquid mass has to vaporize to sustain a cavity. This is the reason why cryogenic fluids are more thermosensitive on the cavitation than water.

Temperature depressions increase as cavitation number σ decreases in Fig. 15. Temperature depressions ΔT near the leading edge are larger than those downstream. The comparison between the cavity aspects in Fig. 14 and the temperature depressions in Fig. 15 shows that the temperature depressions begin to increase rapidly when cavitation clouds with tiny cavity bubbles reach the location of each sensor, respectively. After that, the temperature depressions in cavity region further increase with the expansion of the cavity clouds. The slope of the temperature depression in relation to cavitation number is almost linear. From these measurements, it can be concluded that the temperature depression varies from the inception region of the cavity bubble to the closure region of the cavity clouds, and that the temperature depressions at the bubble growth region, i.e., near the leading edge, are much larger than those at the downstream region. In addition, negative temperature depressions were not observed at all near the cavitation closure where the cavity bubbles disappeared.

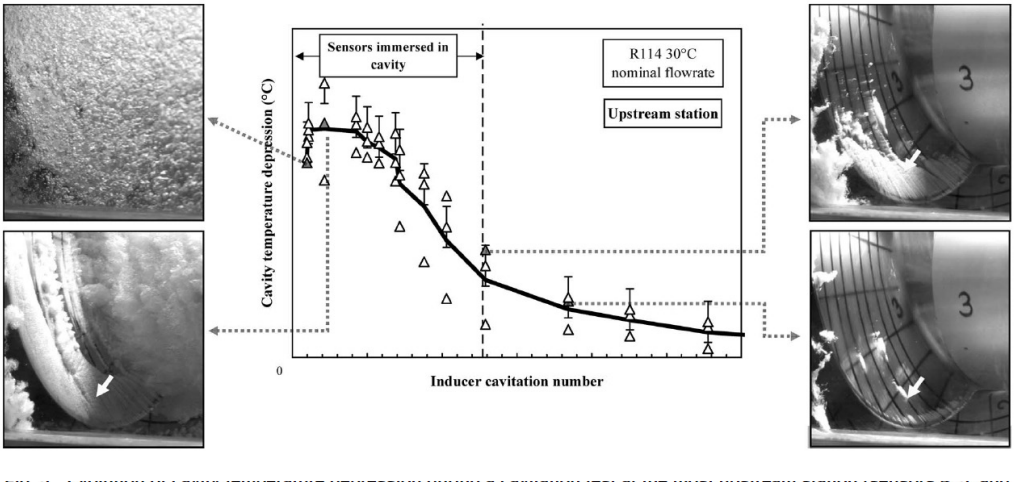

Fig. 11 Evolution of cavity temperature depression during a cavitation test at the most upstream station and correlation with cavity visualizations (R114 at 30℃). The white arrow in picture indicates the location of temperature sensor from [29]

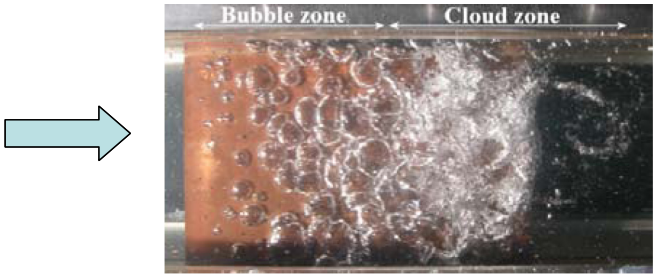

(a) cold water T=25℃ α=4 deg., σ=1.25

(b) hot water T=70℃ α=8 deg., σ=2.0

Fig. 12 Cavitation appearance in (a) cold water T=25℃, α=4 deg., σ=1.25, and (b) hot water T=70℃, α=8 deg., σ=2.0, from [30]

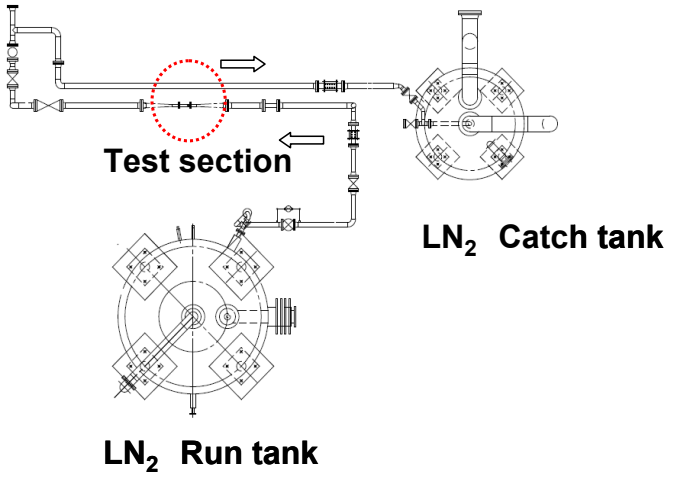

Fig. 13 Cryogenic cavitation tunnel in JAXA from [33]

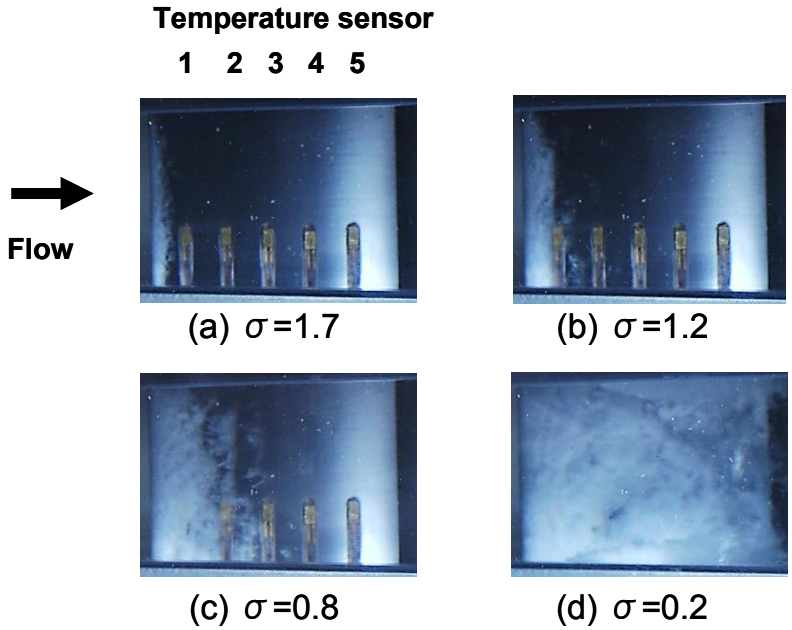

Fig. 14 Aspects of cavitating flow on the hydrofoil (NACA16-012) in liquid nitrogen (90.4 K) at several cavitation numbers for angle of attack 8 degrees

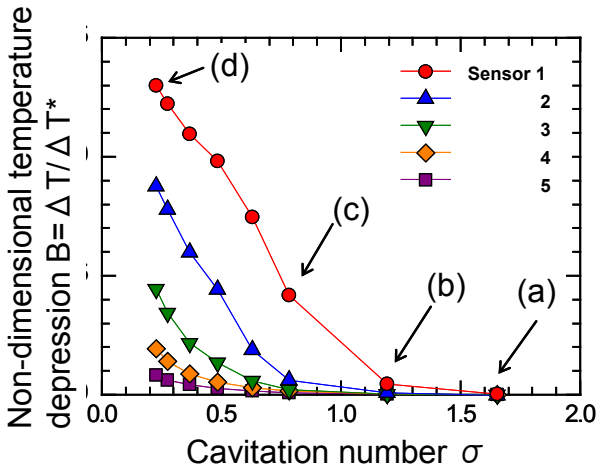

Fig. 15 Non-dimensional temperature depression *B=ΔT/ΔT at each temperature sensor against the cavitation number σ at each diode sensor: (a)-(d) denote the picture number shown in Fig. 14, respectively**

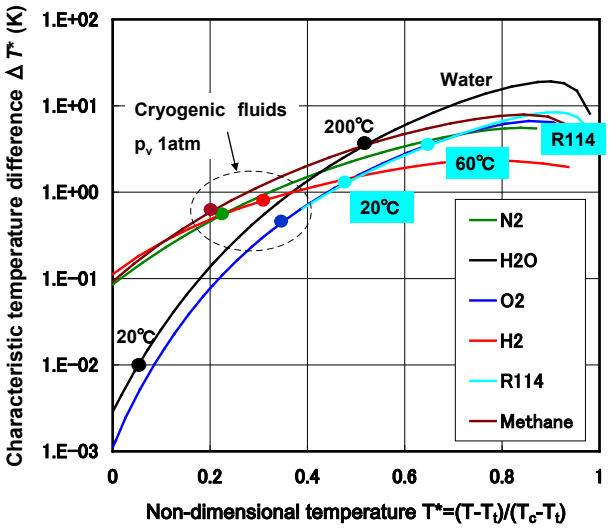

Fig. 16 Variation of the characteristic temperature difference $\Delta T^* = \rho_v L/\rho_l C_{pl}$ of themosensitive fluids compared with water based on the non-dimensional temperature $T^* = (T-T_t)/(T_c-T_t)$

THEORETICAL BACKGROUND

(1) Analysis of thermodynamic effect on cavitation in cryogenic inducer

Watanabe et al. [38] proposed a 2D cascade analysis using the singularity method with consideration of the thermodynamic effect. In his cavitation model, the cavity length is a function of σ/2α (cavitation number/2 x incidence) and the non-dimensional thermodynamic parameter $\Sigma^* = \Sigma\sqrt{C/U^3}$. The degree of the thermodynamic effect is affected by the magnitude of $\Sigma^* = \Sigma\sqrt{C/U^3}$. Brennen's thermodynamic parameter Σ depends only on the fluid temperature. On the other hand, the reference velocity, U (=inducer tip speed), depends on both the inducer rotational speed and inducer diameter, and the chord of blade, C, depends on inducer design, i.e., diameter and solidity. In their analysis, the actual P_v-T curve (non-linear) was applied corresponding to the temperature depression due to the thermodynamic effect instead of the Clapeyron equation in Eq. (3) (linear). The turbulence diffusion factor $\varepsilon=8\times10^3$ to take account of the enhancement of thermal diffusion around the cavity was employed to obtain the reasonable prediction.

Figure 17 shows typical analytical results of the thermodynamic effect on the length of sheet cavitation which presents separately the influence of fluid temperature and rotational speed, i.e., tip velocity, U, on the growth of cavity length L_c/h (L_c is the cavity length, and h is the blade spacing). The growth of cavity length is delayed when the fluid temperature becomes higher and the rotational speed becomes smaller. The delay of the cavitation growth is significant where the cavity length develops over the throat, i.e., L_c/h >1.0. In the case of the half rotational speed (0.5 U), the growth of the cavitation is much suppressed, and head break dose not appear until the lower cavitation numbers. These trends agree well with the previous experimental results for 3D inducers of Franc et al. [9][12] in Fig. 18 and Yoshida et al. [10] in Fig. 19.

Fluid	Temperature	Velocity	Σ *
Water	–	1.0 U	0
Nitrogen	80 K	1.0 U	1.58E+01
Nitrogen	76 K	1.0 U	7.0E+00
Nitrogen	76 K	0.5 U	1.93E+01

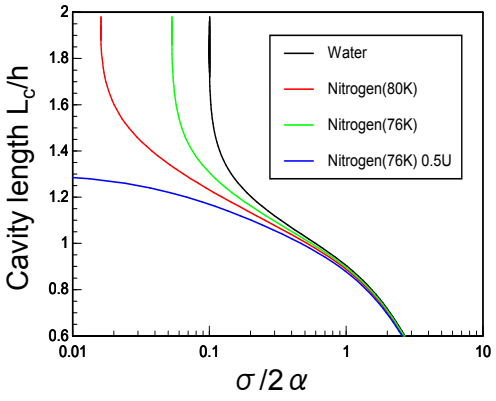

Fig. 17 Analytical results of cavity length in the case of water and liquid nitrogen at 76 K and 80 K, for solidity C/h = 2.0, stagger angle β = 78.8 deg from [38]

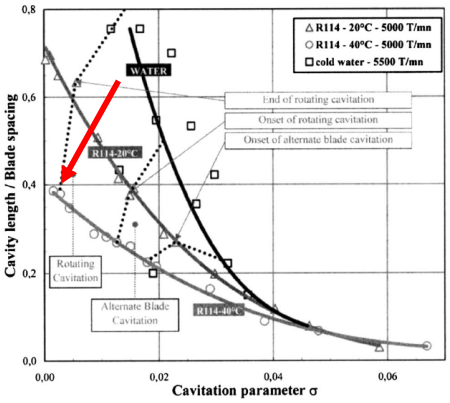

(a) Water and R114 (20 and 40℃) at 5000rpm

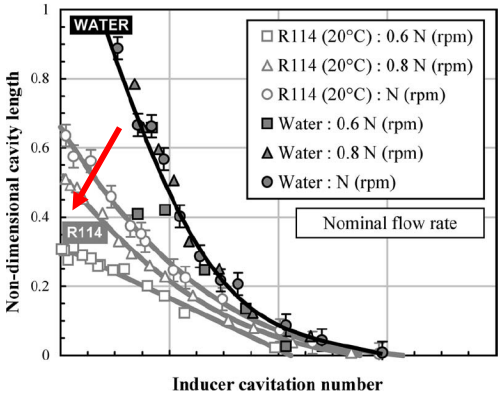

(b) Rotation speed (0.6, 0.8, and 1.0N) for water and R114 at 20℃

Fig. 18 (a) Variation of the cavity length with the cavitation parameter for cold water and for R114 at two different temperatures at 5000 rpm from [9], and (b) Influence of rotation speed (0.6, 0.8, and 1.0N) on cavity length for water and R114 at 20℃ from [12]

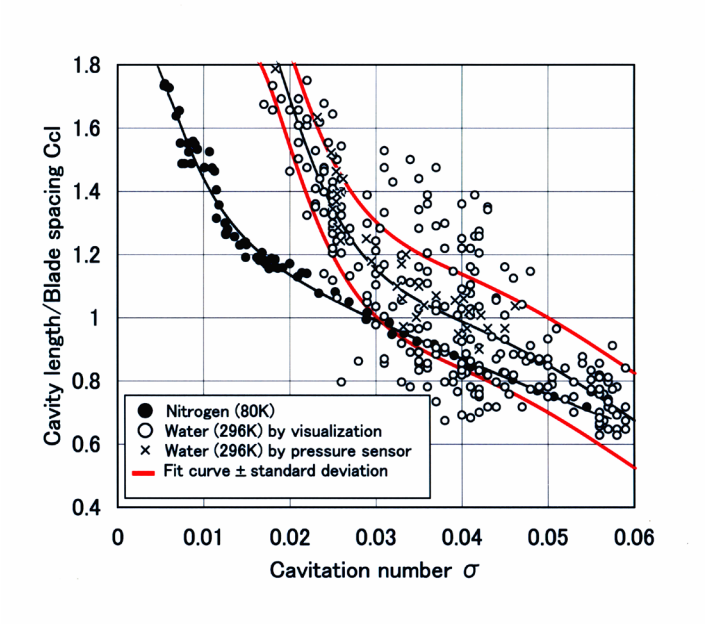

Fig. 19 Comparison of the cavity length of the tip vortex cavitation between in cold water (296 K) and that in liquid nitrogen (80 K) from [10]

(2) Non-dimensional thermodynamic parameter based modified Rayleigh-Plesset equation

In thermosensitive fluid, a decrease of saturated vapor pressure ($\Delta p_v = p_v(T_\infty) - p_v(T_c) = dp_v/dT \cdot \Delta T$), which is caused by temperature depression ($\Delta T = T_\infty - T_c$), delays the growth of cavities. Brennen [4] added a thermal term into the Rayleigh-Plesset equation (Plesset and Zwick [39]) to express this thermal effect. The third term on the left hand side, $dp_v/dT \cdot \Delta T$ in Eq. (2), is the thermal term, and the effects of condensable gas, surface tension, and viscosity are neglected.

$$\rho_l \left[R\ddot{R} + \frac{3}{2}\dot{R}^2 \right] + \frac{dp_v}{dT}\Delta T = p_v(T_\infty) - p \tag{2}$$

where dp_v/dT is the slope of the vapor pressure curve. It can be estimated using Clapeyron's equation in Eq (3). ,

$$\frac{dp_v}{dT} \cong \frac{\rho_v L}{T_\infty} \tag{3}$$

Franc et al. [11] assumed that the heat flux required for phase change is conveyed to the bubble interface by convection. The energy balance on the surface of a cavity is expressed by the following artificial convection heat transfer coefficient h, as shown in Fig. 20.

$$h \cdot \Delta T \cdot 4\pi R^2 = \frac{d}{dt}\left(\frac{4}{3}\pi R^3 \right) \rho_v L \tag{4}$$

Thus,

$$\Delta T = \frac{\rho_v L}{h}\dot{R}$$

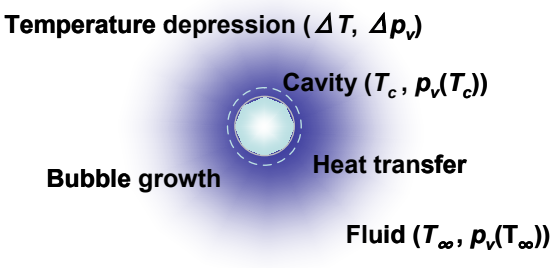

Fig. 20 Heat transfer on the surface of a cavity due to the nature of convection

By introducing this estimate of ΔT in the Rayleigh-Plesset equation (Eq. 2) and making it non-dimensional, the following equation is obtained (Franc et al. [12]).

$$\overline{R}\ddot{\overline{R}}+\frac{3}{2}\dot{\overline{R}}^{2}+\frac{\tau}{\tau_T}\cdot\dot{\overline{R}}=-\frac{C_p+\sigma}{2} \tag{5}$$

where

$$\tau=\frac{C}{U},\quad \tau_T=\frac{Nu\sqrt{\alpha_\ell}}{\Sigma} \tag{6}$$

C is reference length and U is reference velocity, so the unit of τ is time (sec). It is an approximation of transit time of a bubble passing through the inducer blade. Also, the unit of τ_T is time (sec). It can be considered as a characteristic thermal time since it contains flow and heat information from the Nusselt number Nu. Therefore, the non-dimensional thermodynamic parameter τ/τ_T is the ratio of the transit time $\tau = C/U$ and the characteristic thermal time $\tau_T = Nu\sqrt{\alpha_l}/\Sigma$. The thermodynamic effect increases, when the non-dimensional thermodynamic parameter τ/τ_T and the babble growth ratio $\dot{R}$ are large.

The variation of characteristic time $\tau^* = \sqrt{\alpha_l}/\Sigma$ ($\tau_T = Nu\cdot\tau^*$) which depends only on the fluid temperature are presented against the non-dimensional temperature $T^* = (T-T_t)/(T_c-T_t)$ in Fig. 21. Cryogenic fluids or refrigerant R114 are used considerably closer to their critical temperature than cold water. Thus, characteristic times of cryogenic fluids or refrigerant R114 are shorter by several orders of magnitude than that of cold water. The water temperature must be raised to over 150°C to get the same order of the characteristic time τ^* as that of cryogenic fluids.

In the present study, the degree of thermodynamic effect on a cavitating inducer was examined based on non-dimensional thermodynamic parameter τ/τ_T. The relationship of the adjustment of cavitation number $\Delta\sigma$ to the non-dimensional thermodynamic parameter τ/τ_T was examined using the previous two sets of experimental results (Kikuta et al. [15]) as described in next chapter.

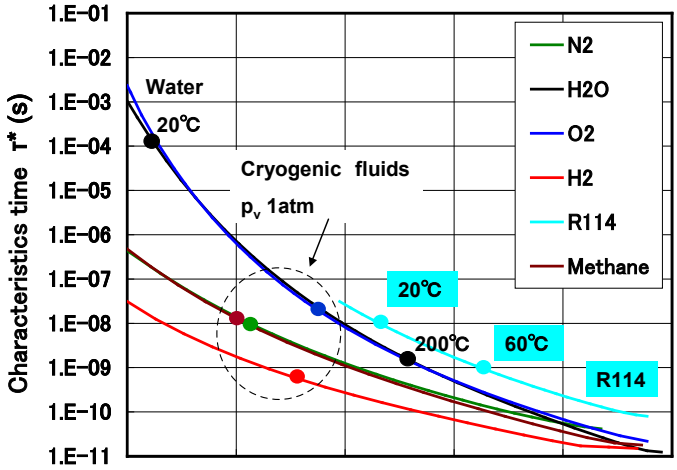

Fig. 21 Variation of the characteristic time τ^*(s) of thermosensitive fluids compared with water based on the non-dimensional temperature $T^* = (T-T_t)/(T_c-T_t)$

EXPERIMENTAL FACILITIES AND PROCEDURE

Experimental facilities

It is well known that a thermal delay of cavitation can occur according to the nature of the fluid. It is almost zero in water at room temperature, but quite significant in cryogenic liquids. Reference tests without the thermodynamic effect were carried out at the Water Inducer Test Facility (WITF) of IHI Corporation shown in Fig. 22. The working fluid was cold water at 306 K after degassing. Dissolved oxygen of the water was 2 ppm due to the degassing process. The rotational speed was N=6000 rpm and the flow rate was $Q/Q_d = 1.0$.

In contrast, a second set of experiments were conducted in liquid nitrogen at the Cryogenic Inducer Test Facility (CITF) of the Japan Aerospace Exploration Agency (JAXA) shown in Fig. 23. The temperature of liquid nitrogen was principally 79 K, and the influence of the bubble nucleus can be almost disregarded in liquid nitrogen. Inducers of the same size and shape (number of blades Z = 3, solidity C/h = 2.0) as those in water were employed in the nitrogen experiments. This geometric similarity ensure the similarity in pressure coefficient C_p of the usual cavitation scaling law. The rotational speed and fluid temperature were varied in order to change the magnitude of thermodynamic effect. Four rotational speeds of N = 18300 rpm, 14000 rpm, 10000 rpm, and 6000 rpm were used with a constant flow rate $Q/Q_d = 1.0$. In addition, a test was conducted in which the temperature of liquid nitrogen was 86 K with a rotational speed of N = 18300 rpm. From these experiments, the difference of the influences on the thermodynamic effect caused by the rotational speeds and fluid temperatures were investigated.

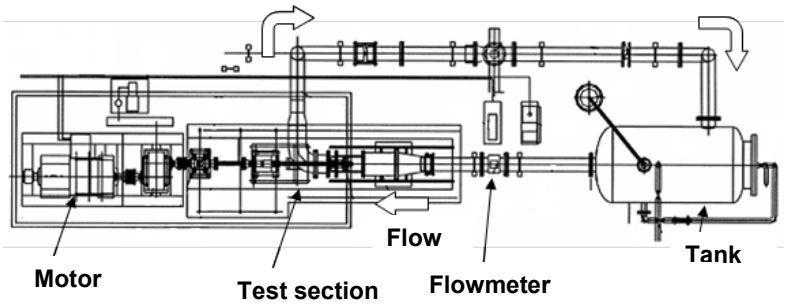

Fig. 22 Water inducer test facility of IHI

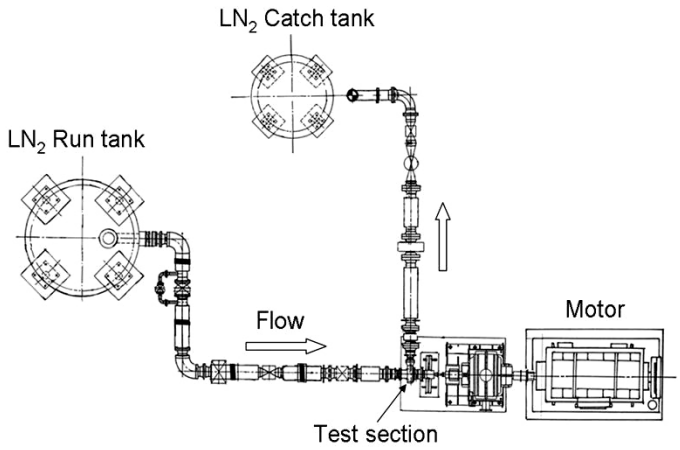

Fig. 23 Cryogenic inducer test facility of JAXA

Experimental procedure

The cavity length L_c of the tip leakage vortex cavitation along the blade was taken to indicate the cavitating situation in the inducer. The cavity length L_c was defined as the length from the leading edge of the blade to the trailing edge of the cavity. In the experiments, the cavitating length L_c was estimated by the same procedure as that employed in previous experiments (Yoshida et al. [40][41]). In both the experiment in cold water and that in liquid nitrogen, the cavitating region was estimated based on the pressure distribution, which was measured by pressure sensors installed on the casing. Figure 24 shows the location of the pressure taps (Pos. 1-8) in the experiments. There are eight sensors located from the leading edge to the trailing edge along the blade. Using the pressure wave forms measured by eight pressure sensors at each location, contour plots describing the cavitation state in the blade channel. Figure 25 is drawn by rearrangement of the wave forms of all the sensors. The blue area shows “estimated cavity region.” We defined the length from the leading edge to the trailing edge of the estimated cavity region as cavity length (L_c). In other words, the length of the blue region along the blade in Fig. 25 is the cavity length. In the previous work (Yoshida et al. [10]), results of this indirect visualization using the pressure sensors agreed with direct optical observation results in water.

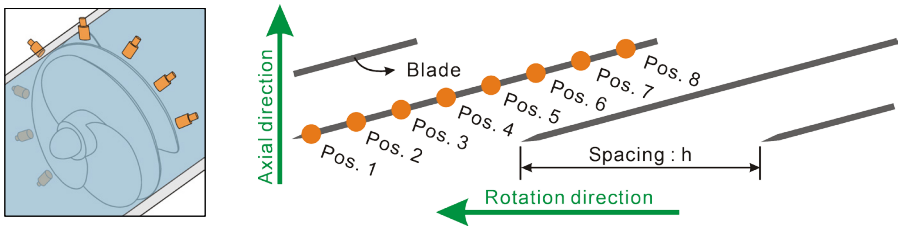

Fig. 24 Location of pressure taps along the blade for measurements of cavity length

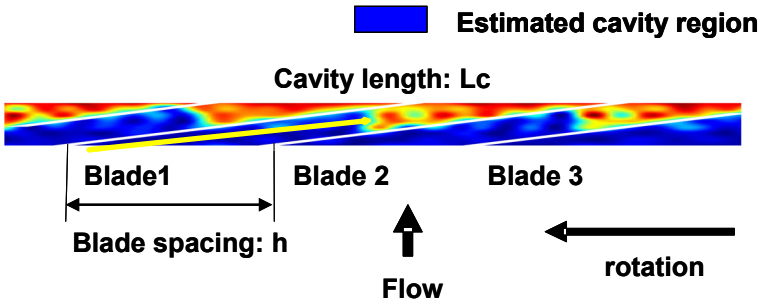

Fig. 25 Example of estimated cavity region obtained from the measured pressure distribution

EXPERIMENTAL RESULTS

Figure 26 shows comparisons of the cavitation performances and the cavity length estimated from the pressure distribution in cold water (○,◇) with those in liquid nitrogen (79K / 18300 rpm (○, ◇), 79 K/14000 rpm (○,◇), 79 K/10000 rpm (○,◇), and 86 K/18300 rpm (○,◇)) (Kikuta et al. [15]). The horizontal axis is the cavitation number ratio σ/σ_0, where σ_0 is the head break cavitation number of the experiment in cold water. The vertical axis on the left side is the normalized head coefficient ψ/ψ_o, and that on the right side is the cavity length C_{cl} (= L_c/h, L_c is cavity length along the blade from the leading edge of the blade to the trailing edge of the cavity, and h is blade spacing).

Before the head break, the cavity length C_{cl} increases almost linearly with the decrease of the cavitation number. Compared with the experiments in liquid nitrogen at the same cavitation number, the cavity length became predictably shorter, when the rotational speed decreased. In all of the experiments, the cavity length C_{cl} grew rapidly (“jump”) in the same C_{cl} region from 1.35 to 1.70, and the head break

occurred concurrently. Since this C_{cl} region was unrelated to the experimental conditions such as fluid, rotational speed, and temperature, this "jump" is considered to be a characteristic of the inducer design which was employed in these experiments. On the other hand, the cavitation numbers when the "jump" of cavity length occurred differed according to the experimental conditions. Thus, the thermodynamic effect in the inducer appeared due to the suppression of cavity length, resulting in improvement of the cavitation performance.

Cavitation performance was greatly improved in liquid nitrogen. In addition, when the rotational speed decreased or the fluid temperature increased in liquid nitrogen, the head break cavitation numbers shifted to the left. The influence of rotational speed and fluid temperature on the thermodynamic effect resulted in improvement of cavitation performance.

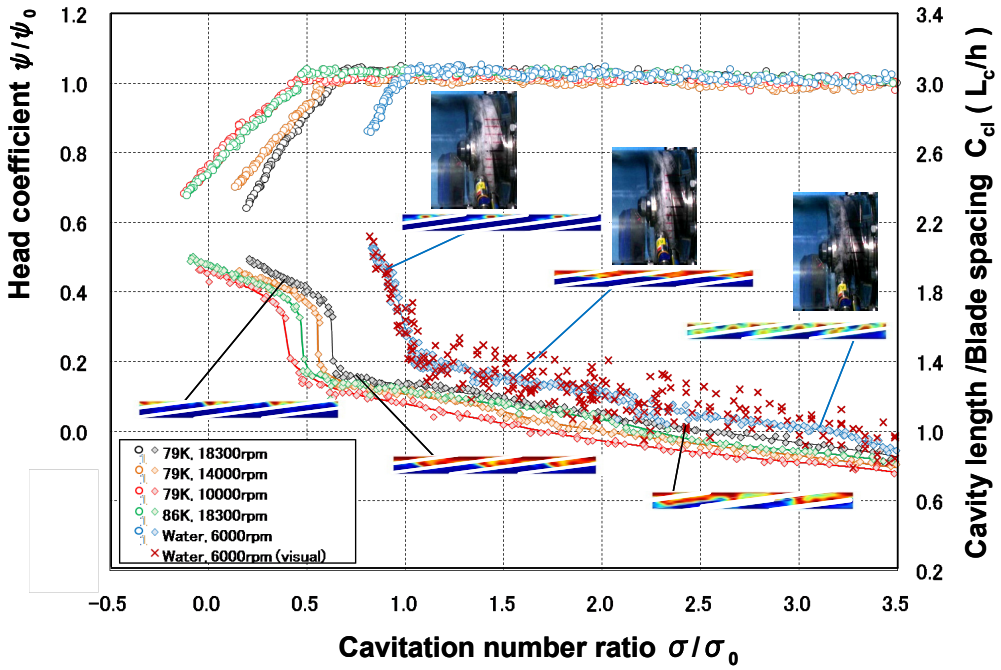

Fig. 26 Cavitation performance, pressure coefficient and cavity length in cold water and in liquid nitrogen for several rotational speeds and temperatures from [15]

DISCUSSIONS

Non-dimensional thermodynamic parameter τ/τ_T

In pump engineering, the thermodynamic effect on pump cavitation performance is conventionally understood as the increase of the adjustment of cavitation number $\Delta\sigma = \sigma_c - \sigma$ (σ_c is the cavitation number in the absence of any thermal effect, and σ is the cavitation number in thermosensitive fluid) at which the same cavitation phenomena (e.g., cavitation inception point, onset of the cavitation instabilities, and head

break point) occur. The influence of rotation speed (Ω) and liquid temperature (T_∞) on the adjustment of the cavitation number ($\Delta\sigma$) is analyzed on the basis of the ratio of two times, namely, the transit time, τ, and the characteristic thermodynamic time, τ_T .

Experimental conditions of the inducer are summarized in Table 1. To obtain the non-dimensional thermodynamic parameters τ/τ_T in Table 1, Nusselt number *Nu* should be defined to calculate τ_T. However, the heat transfer coefficient on the interface of cavitation has not yet been clarified. Unfortunately, these are the most difficult parameters to evaluate the heat transfer coefficient at the cavity interface.

Under the present experimental conditions, the heat transfer at the interface of the cavity is assumed to be forced-convection heat transfer with strong turbulent flow. In this condition, the Nusselt number *Nu* is presented in the form of a product of Reynolds number *Re* and Prandtl number *Pr*. Some empirical formulae about Nusselt number *Nu(Re, Pr)* have been suggested based on experimental results. In these empirical equations, the Reynolds number, *Re*, influences the Nusselt number, *Nu*, by about 0.8^{th} power. Therefore, the influence of the rotational speed on the Nusselt number *Nu* does not change so much regardless of which equation is applied. Colburn's equation [42], which is used to calculate the heat transfer between the liquid and inner surface of circular pipe, is one of the most general equations, expressed as follows:

$$Nu = 0.023 \times \mathrm{Re}^{0.8} \times \mathrm{Pr}^{\frac{1}{3}} \tag{7}$$

where

$$\mathrm{Re} = \frac{UC}{\nu}, \quad \mathrm{Pr} = \frac{\nu}{\alpha_l}$$

Supposedly, the Colburn equation can be applied to calculate the Nusselt number *Nu* of the present experimental conditions, although this application seems to be a bold assumption.

In Table 1, the non-dimensional thermodynamic parameter τ/τ_T in the experiment in water is $0.01 << 1$ and that in liquid nitrogen is $2\text{-}15 > 1$. Thus, the time until a cavity passes through the inducer (transit time τ) is sufficiently greater than the characteristic thermal time (τ_T) in the experiment in liquid nitrogen. Figure 27 shows cavitation number ratio σ/σ_0 when the cavitation length C_{cl} grows to 1.4 (= head break point of the present inducer) against the non-dimensional thermodynamic parameter τ/τ_T . Because the vertical axis in Fig. 27 is expressed based on the cavitation number σ_0 when the cavitation length C_{cl} grows to 1.4 in the water experiment without the thermodynamic effect, the value $1.0\text{-}\sigma/\sigma_0$ is equal to the increase of the cavitation number $\Delta\sigma/\sigma_0$ as an adjustment caused by the thermodynamic effect. It can be seen that the cavitation number ratio σ/σ_0 when the cavity length C_{cl} grows to 1.4 was decreased with decreasing rotational speed and increasing fluid temperature. The cavitation number ratio σ/σ_0 of the experimental results with decreasing rotational speed decreases regularly along with the non-dimensional

thermodynamic parameter τ/τ_T. The increase of the cavitation number $\Delta\sigma/\sigma_0$ results in good correction by non-dimensional thermodynamic parameter τ/τ_T.

Here, peripheral speed of inducer tip U influences the non-dimensional thermodynamic parameter τ/τ_T by -1.8th power in the present analysis. However, the heat transfer on the interface of cavitation has not yet been clarified. Thus, more investigation is needed to apply the equation to define the Nusselt number.

In addition, the other example of the thermodynamic parameter τ/τ_T shows in Fig. 28. For LOX turbopump of J-2 Engine, cavitation performance data with various temperatures (90 K to 101 K) from NASA TN D-7451 [43] were rearranged by the proposed thermodynamic parameter τ/τ_T. The trends of Fig. 27 and Fig. 28 are very similar, both figures show the good relation between the adjustment of cavitation number σ/σ_o to the thermodynamic parameter τ/τ_T. However, there is the difference of the slope against the thermodynamic parameter τ/τ_T between in Fig. 27 and Fig. 28. This reason can be explained by the analytical results of Watanabe's 2D cavitating cascade with consideration of the thermodynamic effect [44]. Figure 29 show the cavitation number ratio σ/σ_0 (σ_0 is the cavitation number in the absence of any thermal effect, and σ is the cavitation number in thermosensitive fluid) versus the thermal effect parameter Σ^* in Eq. (1) with the cavitation length L_c/h (C_{cl})= 0.6, 1.0, 1.4. It was found that the slope is depended on the cavity length L_c/h as the cavitation parameter (indication). When the cavity length is shorter (i.e., L_c/h (C_{cl})= 0.6), the slope is smaller. However, when the cavity length is larger (i.e., L_c/h (C_{cl})=1.4), the slope is larger. From these analytical results, the difference of the slope between in Fig. 27 and Fig. 2 8 is caused by the cavitation performance of the inducers based on the cavity length at the head break. In other words, the inducer in Fig. 27 has the high cavitation performance, but the inducer in Fig. 28 not so good one. The reason was seemed to be the difference of the blade design of new age in JAXA (in Fig. 27) and old age in NASA (in Fig. 28).

Note) The difference between 76k (blue line) and 80K (red line) in Fig. 28 is caused by the non-linear effect of dp_v/dT (i.e., the slope of the vapor pressure curve). Clapeyron's equation in Eq. (3) was not used in Watanabe's thermodynamic model [38].

Table 1 Comparisons of the thermodynamic parameter τ/τ_T

Fluid	Temperature T (K)	Rotational speed N (rpm)	Thermodynamic function Σ (m/sec$^{3/2}$)	Non-dim. thermodynamic parameter Σ^*	Nusselt number Nu	Thermal time τ_T (sec)	Transit time τ (sec)	Time ratio τ/τ_T
Water	306	6000	1.62E+01	2.87E-02	2.64E+04	6.30E-01	6.74E-03	1.07E-02
Nitrogen	79	6000	4.00E+04	7.10E+01	6.26E+04	4.37E-04	6.74E-03	1.54E+01
Nitrogen	79	10000	4.00E+04	3.30E+01	9.41E+04	6.57E-04	4.05E-03	6.15E+00
Nitrogen	79	14000	4.00E+04	1.99E+01	1.23E+05	8.61E-04	2.89E-03	3.36E+00
Nitrogen	79	18300	4.00E+04	1.33E+01	1.53E+05	1.07E-03	2.21E-03	2.07E+00
Nitrogen	86	18300	1.42E+05	4.74E+01	1.74E+05	3.25E-04	2.21E-03	6.81E+00

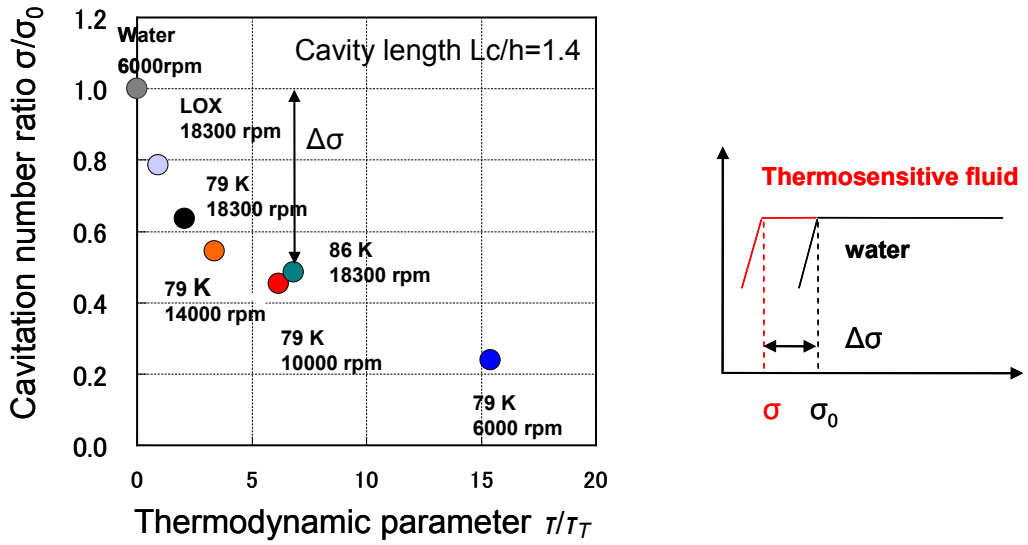

Fig. 27 Influence of thermodynamic parameter τ/τ_T on cavitation number σ at which the cavity length is Lc/h=1.4 (head break point of the present inducer)

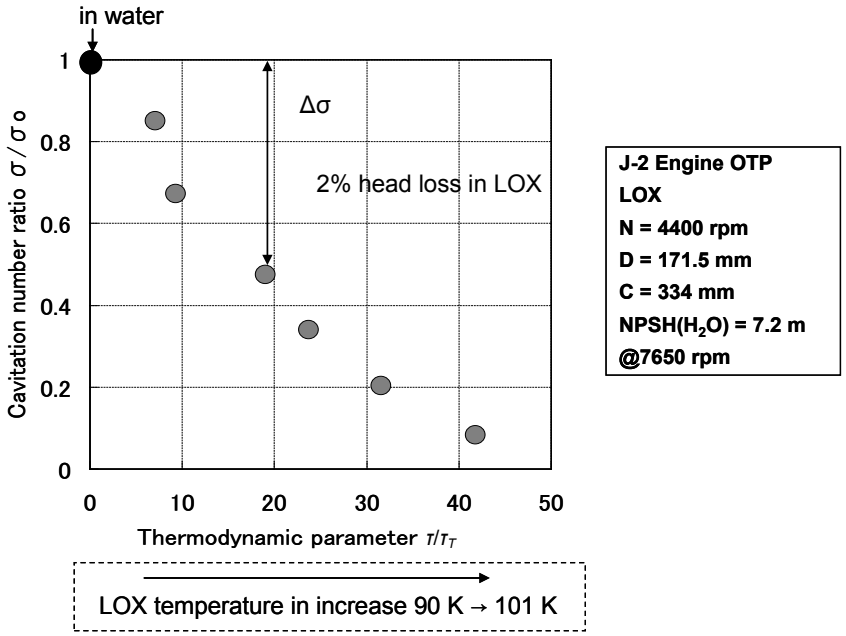

Fig. 28 Influence of thermodynamic parameter τ/τ_T on cavitation number σ at which the head loss is 2%

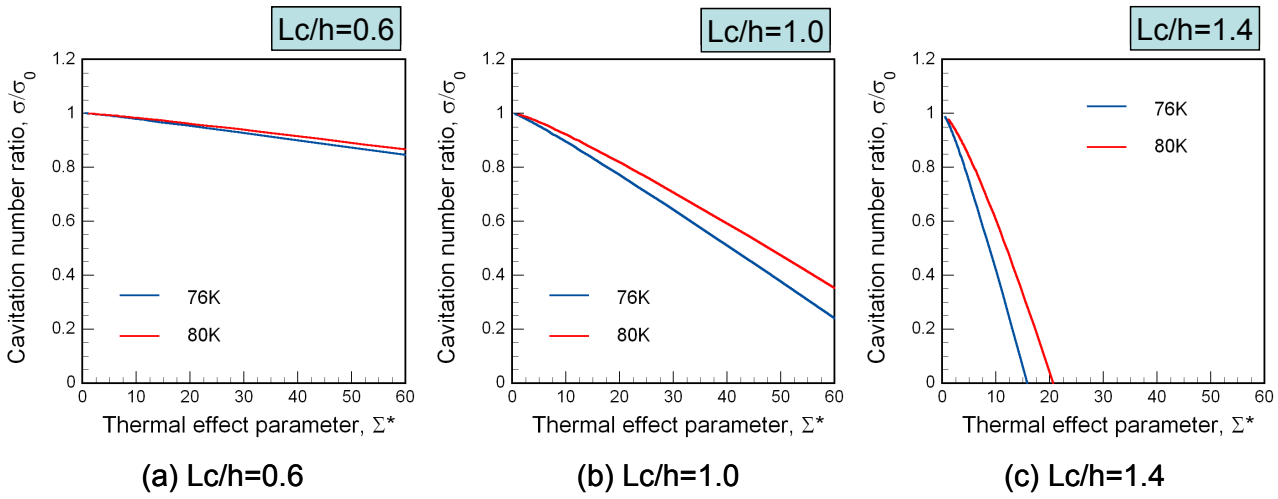

Fig. 29 Influence of thermodynamic parameter Σ^* on cavitation number σ at which the cavitation length is (a) Lc/h=0.6, (b) Lc/h=1.0, and (c) Lc/h=1.4, for liquid nitrogen at T=76 K and 80 K from [44]

Scaling law with thermodynamic effect

From the modified Rayleigh-Plesset equation with the thermal term (Eq. (5)), scaling laws to be satisfied between two different flows are considered in order to ensure similar cavity growth with the thermal effect.

(1) First, the geometric similar is necessary in order to ensure similarity in pressure coefficient distribution C_p on the right hand side of Eq. (5). In other words, since the pressure coefficient distribution C_p depends on the inducer blade design, the design parameters of the blade (incidence, solidity, blade camber, swept back, tip clearance, hub/tip ratio, inlet flow coefficient et al.) must remain the same.

(2) The similarity of usual scaling law in cavitation number, σ, is also necessary to keep the term on the right hand side of Eq. (5). In other words, inlet cavitation number σ depends on the inducer operation condition.

These are basically the usual cavitation scaling law in the absence of any thermal effect.

(3) An additional scaling law is necessary for the cavity growth with the thermodynamic effect. Bubbles will develop similarly when the value of the non-dimensional thermodynamic parameter τ/τ_T in the thermal term on the left hand side of Eq. (5) remains the same.

(4) The amplitude of the thermodynamic effect depends upon the ratio τ/τ_T of the transit time to the characteristic thermodynamic time. In other words, transit time, τ, depends on inducer size and rotational speed, and the characteristic thermodynamic time, τ_T, depends on the fluid property and operating temperature, as shown in Fig. 27. Also, the nature of the heat transfer at the interface of the cavity is also important. As this thermodynamic parameter τ/τ_T becomes larger, the degree of the adjustment of cavitation number, $\Delta\sigma/\sigma_0$, becomes larger.

Figure 30 shows the relation of the cavitation parameters with the involved factors.

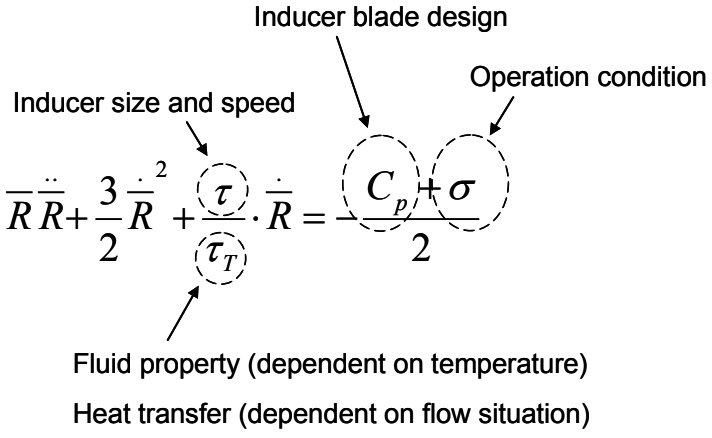

Fig. 30 Cavitation parameters considered for cavity growth with thermal effect

CONCLUDING REMARKS

To obtain a fundamental understanding of the effect of the thermodynamic parameter on cavitation in inducer, two sets of experiments were conducted with liquid nitrogen.

First, the aspects of the cavitation in the inducer were observed by direct optical visualization in liquid nitrogen. The cavity consisted of fine bubbles which seem to be “creamy” in liquid nitrogen as opposed to “icy” in water. Furthermore, it could be observed that the cavity length in liquid nitrogen was shorter than that in water. In addition, the temperature depression of the cavity on the hydrofoil due to the thermodynamic effect was measured in liquid nitrogen. The temperature depression varied from the inception region of the cavity bubble to the closure region of the cavity clouds. The temperature depression at the bubble growth region, i.e., near the leading edge, was much larger than that in the downstream region. Negative temperature depression was not observed at all near the cavitation closure. On the other hand, the cavity length did not oscillate when the cavity length developed over a chord of 0.5-0.7C. Cavitation instabilities caused by the re-entrant jet were perfectly suppressed due to the thermodynamic effect.

Second, joint experiments in liquid nitrogen and cold water were conducted on the cavitaing inducer. In nitrogen experiments, operating conditions, i.e., rotational speed, Ω, and liquid temperature, T_∞, were varied to determine the cavitation scaling law. Through these experimental results, the characteristics times, namely, the transit time, $\tau=C/U$, for bubble growth and the characteristic thermal time, $\tau_T = Nu\sqrt{\alpha_l}/\Sigma$, introduced from the thermal property, were investigated as a cavitation thermodynamic parameter. It was confirmed that the adjustment cavitation number, $\Delta\sigma/\sigma_0$, has a good correlation with the non-dimension thermodynamic parameter τ/τ_T, which is the ratio of the transit time and the characteristic thermal time. However, the degree of the heat transfer at the interface of the cavity bubble depends on the situation of the flow, and it consequently influences the degree of the thermodynamic effect through the cooling of the temperature. A more sophisticated heat transfer model on the interface of the cavity bubble is needed to clarify the thermodynamic effect on cavitation.

ACKNOWLEDGEMENT

The great help and many fruitful discussions by Dr. Hiroharu Kato are gratefully acknowledged. His insights into this problem were invaluable to our effort. The authors would like to thank IHI Corporation, which allowed use of the experimental data, and Mr. Satoshi Kawasaki of IHI Corporation, who gave valuable advice.

NOMENCLATURE

B : Stepanoff's B-factor $=V_v/V_l=\Delta T/\Delta T^*$

C : chord of blade

C_{cl} : cavity length / blade spacing $= L_c/h$

C_p : pressure coefficient

C_{pl} : specific heat of liquid

h : blade spacing
or convention heat transfer coefficient

L : latent heat of vaporization

L_c : cavity length

N : rotational speed

Nu : Nusselt number

Pr : Prandtl number $= \nu/\alpha_l$

p_v : vapor pressure

Q : flow rate

Q_d : design flow rate

q : heat flux

R : bubble radius

Re : Reynolds number $= UD/\nu$

R_T : inducer radius

T_c : cavity temperature
or temperature of critical point

T_t : temperature of triple point

T_∞ : liquid temperature at infinity

T^* : non-dimensional temperature $= (T-T_t)/(T_c-T_t)$

ΔT : temperature difference

ΔT^* : characteristic temperature difference $= \rho_v L/\rho_l C_{pl}$

t : time

t_c : critical thermal time

U : peripheral speed of inducer tip
or reference velocity

V_l : volume flow rate of liquid

V_v : volume flow rate of vapor

Y : Kato's Y-factor $= \alpha\sqrt{C/U^3}$

Z : number of blades

α : Kato's thermodynamic parameter $= \sqrt{\rho_l / \rho_v}\,\Sigma$
or incidence

α_l : thermal diffusivity of liquid

β : stagger angle

ε : turbulence diffusion factor

ν : kinematic viscosity

ρ_l : liquid density

ρ_v : vapor density

λ_l : liquid thermal conductivity

Σ : Brennen's thermodynamic parameter defined by Eq. (1)

Σ^* : Watanabe's non-dimensional thermodynamic parameter $= \Sigma\sqrt{C/U^3}$

Σ^{**} : Brennen's modified non-dimensional thermodynamic parameter $= \Sigma \Big/ \left\{R_T{}^2\Omega^3\phi(\sigma_x)_0\right\}^{\frac{1}{2}}$

σ : cavitation number

σ_c : cavitation number in the absence of any thermal effect

σ_o : cavitation number when the cavitation length is C_{cl} =1.4 in water

$\Delta\sigma$: adjustment of cavitation number $= \sigma_c - \sigma$

σ_x : head break cavitation number in thermosensitive fluid

$(\sigma_x)_0$: head break cavitation number in the absence of any thermal effect

τ : transit time $=C/U$,

τ_T : characteristic thermal time $= Nu\sqrt{\alpha_l}\,/\,\Sigma$

τ^* : characteristic time $= \sqrt{\alpha_l}\,/\,\Sigma$

τ/τ_T : Franc's non-dimensional thermodynamic parameter

ϕ : coefficient of flow rate

Ψ : head coefficient

Ψ_o : normal head coefficient

Ω : rotational angular speed

REFERENCES

[1] Stepanoff, A. J., 1964, "Cavitation Properties of Liquids," ASME Journal of Engineering for Power, **86**, pp. 195-200.

[2] Cooper, P., 1967, "Analysis of Single- and Two-Phase Flows in Turbopump Inducers," ASME Journal of Eng. for Power, **89** (4), pp. 577-588.

[3] Stahl, H. A., Stepanoff, A. J., and Phillipsburg, N. J., 1956, "Thermodynamic Aspects of Cavitation in Centrifugal Pumps," ASME J. Basic Eng., **78**, pp. 1691-1693.

[4] Brennen, C. E., 1973, "The Dynamic Behavior and Compliance of a Stream of Cavitating Bubbles," ASME Journal of Fluids Eng., **95** (4), pp. 533-541.

[5] Brennen, C. E., 1994, "Hydrodynamics of Pumps," Concepts FTI, Inc. and Oxford University Press, pp. 142-149.

[6] Kato, H., 1984, "Thermodynamic Effect on Incipient and Developed Sheet Cavitation," International Symposium on Cavitation Inception, ASME FED-Vol.16., New Orleans, L. A., 9-14 December, pp. 127-136.

[7] Hord, J., Anderson, L. M., and Hall, W. J., 1972, "Cavitation in Liquid Cryogens Volume I - Venturi," constructor report-2054, NASA., Hord, J., 1973, "Cavitation in Liquid Cryogens Volume II - Hydrofoil," constructor report-2156, NASA., Hord, J., 1973, "Cavitation in Liquid Cryogens Volume III - Ogives," constructor report-2242, NASA.

[8] Watanabe, S., Hidaka, T., Horiguchi, H., Furukawa, A., and Tsujimoto, Y., 2007, "Analysis of Thermodynamic Effects on Cavitation Instabilities," ASME Journal of Fluids Eng., **129** (9), pp. 1123-1130.

[9] Franc J. P., Rebattet C., and Coulon A., 2004, "An Experimental Investigation of Thermal Effects in a Cavitating Inducer," ASME Journal of Fluids Eng., **126** (5), pp. 716-723.

[10] Yoshida, Y., Kikuta K., Hasegawa S., Shimagaki M., and Tokumasu T., 2007, "Thermodynamic Effect on a Cavitating Inducer in Liquid Nitrogen," ASME Journal of Fluids Eng., **129** (3), pp. 273-278.

[11] Franc J. P., and Pellone C., 2007, "Analysis of Thermal Effects in a Cavitating Inducer Using Rayleigh Equation," ASME Journal of Fluids Eng., **129** (8), pp. 974-983.

[12] Franc, J. P., Boitel G., Riondet, M., Janson, E., Ramina, P., and Rebattet, C., 2010, "Thermodynamic Effect on a Cavitating Inducer-Part I: Geometrical Similarity of Leading Edge Cavities and Cavitation Instabilities," ASME Journal of Fluids Eng., **132** (2), pp. 021303-1-021303-8.

[13] Cervone A., Testa R., and d'Agostino L., 2005, "Thermal Effects on Cavitation Instabilities in Helical Inducers," AIAA Journal of Propulsion and Power, **21** (5), pp. 893-899.

[14] Kikuta, K., Yoshida, Y., Watanabe, M., Hashimoto, T., Nagaura, K., and Ohira, K., 2008, "Thermodynamic Effect on Cavitation Performances and Cavitation Instabilities in an Inducer," ASME Journal of Fluids Eng., **130** (11), pp. 111302-1-11302-8.

[15] Kikuta, K., Yoshida, Y., Hashimoto, T., Hanri, H., Mizuno, T., and Shimiya, N., 2009, "Influence of Rotational Speed on Thermodynamic Effect in a Cavitating Inducer," Proceeding of ASME Fluids Enginenering Division Summer Meeting, FEDSM2009-780823, 2-6 August, Vail, Colorado, USA.

[16] Yoshida, Y., Nanri, H., Kikuta, K., Kazami, Y., Iga, Y., and Ikohagi, T., 2009, "Influence of Thermodynamic Effect on Sub-synchronous Rotating Cavitation," JAXA Research and Development Memorandum, JAXA-RM-09-005.

[17] Hosangadi A., Ahuja V., Ungewitter, R., and Busby, J., 2007, "Analysis of Thermal Effects in Cavitating Liquid Hydrogen Inducers," J. of Propulsion and Power, **23**, No. 6, pp. 1225-1234.

[18] Ball, C. l., Meng, P. R., and Reid, L., 1967, "Cavitation performance of 84^o Helical Pump Inducer Operated in 37^{o}R and 42^{o}R Liquid Hydrogen," NASA Report No. TM X-1360.

[19] Goncalves, E., Pateiia, R., F., Rolland, J., Pouffary, B., and Challier, G., 2010, "Thermodynamic Effect on a Cavitating Inducer in Liquid Hydrogen," ASME, J. of Fluids Eng., **132**(11), pp. 111305-1-111305-7.

[20] Meng, P. R., and Moore, R. D., 1970, "Hydrogen Cavitation performance of 80.6^o Helical Inducer Mounted in Line With Stationary Centerbody," NASA Report No. TM X-1935.

[21] Watanabe, M., Nagaura, L., Hasegawa, S., Niiyama, K., Yoshida, Y., and Sugita, E., 2010, "Direct Visualization for Cavitating Inducer in Cryogenic Flow (The 3rd report: Visual Observations of Cavitation in Liquid Nitrogen)," (in Japanese) JAXA Research and Development Memorandum, JAXA-RM-09-010.

[22] Sarosdy L. R. and Acosta, A. J., 1961, "Note on Observations of Cavitation in Different Fluids," ASME, J. of Basic Enginenering, **83**, pp. 399-400.

[23] Hosangadi A., and Ahuja V., 2005, "Numerical Study of Cavitation in Cryogenic Fluids," ASME, J. of Fluids Eng., **127** (2), pp. 267-281.

[24] Horiguchi, H., Watanabe, S., Tsujimoto, Y., and Aoki, M., "A Theoretical Analysis of Alternate Blade Cavitation in Inducers," 2000, ASME Journal of Fluids Eng., **122** (1), pp. 156-163.

[25] Iga, Y., Nohmi, M., Goro, A., and Ikohagi, T., 2004, "Numerical Analysis of Cavitation Instabilities Arising in the Three-Blade Cascade," ASME Journal of Fluids Eng., **126** (3), pp. 419-429.

[26] Iga, Y., and Yoshida, Y., 2011, "Mechanism of Propagation Direction of Rotating Cavitation in a Cascade," AIAA Journal of Propulsion and Power, **27 (3)**, pp. 675-683.

[27] An, B., Kajishima, T., and Okabayashi, K., 2009, "Generality of Rotating Partial Cavitation in Two-Dimensional Cascades," Proceedings of the 7th International Symposium on Cavitation CAV2009, Paper No.90, 17-22 August, Michigan.

[28] Tani, N., Yamanishi, N., and Tsujimoto, Y., 2012, "Influence of Flow Coefficient and Flow Structure on Rotational Cavitation in Inducer," ASME Journal of Fluids Eng., **134** (2), pp. 021302-1-021302-13.

[29] Franc, J. P. , Boitel G., Riondet, M., Janson, E., Ramina, P. and Rebattet, C., 2010, "Thermodynamic Effect on a Cavitating Inducer-Part Ⅱ: On-Board Measurements of Temperature Depression Within Leading Edge Cavities," ASME, J. of Fluids Eng., **132**(2), pp. 021304-1-021304-9.

[30] Cervone, A., Bramanti, C., Rapposelli, E., and d'Agostino, L., 2006, "Thermal Cavitation Experiments on a NACA 0015 Hydrofoil," ASME Journal of Fluids Eng., **128** (3), pp. 326-331.

[31] Gustavsson, J. P. G., Denning, K. C., and Segal, C., 2008, "Hydrofoil Cavitation Under Strong Thermodynamic Effect," ASME Journal of Fluids Eng., **130** (9), pp. 091303-1-091303-5.

[32] Niiyama, K., Yoshida, Y., Hasegawa, S., Watanabe, M., and Oike, M., 2012, "Experimental Investigation of Thermodynamic Effect on Cavitation in Liquid Nitrogen," Proceedings of the 8th International Symposium on Cavitation CAV2012, Paper No. 231, pp. 153-157, 14-16 August, Singapore.

[33] Niiyama, K., Yoshida, Y., Hasegawa, S., Watanabe, M., Hashimoto, T., Shimgaki, M., Kikuta, K., Nagaura, K., and Tamura, T., 2009, "Verification Test Results of the Cryogenic Cavitation Tunnel in JAXA," (in Japanese) JAXA Research and Development Memorandum, JAXA-RM-08-008.

[34] Franc, J. P., and Michel, M., 1985, "Attached Cavitation and the Boundary Layer: Experimental Investigation and Numerical Treatment," J. Fluid Mech. **154,** pp.63-90.

[35] Kawakami, Y., Kato, H., Yamaguchi, H., Tanimura, M., and Tagaya, Y., 1997, "Mechanism and Control of Cloud Cavitation," ASME Journal of Fluids Eng., **119** (4), pp. 788-794.

[36] Watanabe, S., Konishi, Y., Nakamura, I., and Furukawa, A., "Experimental Analysis of Cavitating Behavior Around a Clark Y Hydrofoil," 2011, WIMRC 3rd International Cavitation Forum 2011, 4-6 July, University of Warwick, UK.

[37] Dr. Hiroharu Kato, 2011, Private letter

[38] Watanabe, S., Furukawa, A., Yoshida, Y., 2008, "Theoretical Analysis of Thermodynamic Effect of Cavitation in Cryogenic Inducer Using Singularity Method," International Journal of Rotating Machinery, Vol. 2008, Article ID 125678.

[39] Plesset, M. S., and Zwick, S. A., 1954, "The Growth of Vapor Bubbles in Super-heated Liquids," J. of Applied Physics, **25**, No.4, pp. 493-500.

[40] Yoshida, Y., Sasao, Y., Watanabe, M., Hashimoto, T., Iga, Y., and Ikohagi, T., 2009, "Thermodynamic Effect on Rotating Cavitation in an Inducer," ASME Journal of Fluids Eng., **131** (9), pp. 091302-1-091302-7.

[41] Yoshida, Y., Nanri, H., Kikuta K., Kazami, Y., Iga, Y., and Ikohagi, T., 2011, "Thermodynamic Effect on Subsynchronous Rotating Cavitation and Surge Mode Oscillation in a Space Inducer," ASME Journal of Fluids Eng., **133** (6), pp. 061301-1-061301-7.

[42] Colburn, A. P., 1933, "A Method of Correlating Forced Convection Heat Transfer Data and a Comparison with Fluid Friction," American Institute of Chemical Engineers, **29**, pp. 174-210.

[43] Gross, Loren A., 1973, An Experimental Investigation of Two-phase Liquid Oxygen Pumping," NASA TN D-7451.

[44] Dr. Satoshi Watanabe, 2010, Private letter